Available online at www.sciencedirect.com

ScienceDirect

Procedia CIRP 129 (2024) 145–150

www.elsevier.com/locate/procedia

18th CIRP Conference on Computer Aided Tolerancing (CAT2024)

The X-ray computed tomography simulation in geometric metrology: a review and case study

Wuzhen Huang*, Huan Shao, Stefano Petrò, Giovanni Moroni

Department of Mechanical Engineering, Politecnico di Milano, Via La Masa 1, 20156, Milano, Italy

* Corresponding author. Tel.: +39-022-399-8575; *E-mail address:* Wuzhen.huang@polimi.it

Abstract

Industrial X-ray computed tomography (XCT) has gained attention in geometric metrology for its ability to scan objects with diverse internal and external features simultaneously. However, challenges persist in inspection planning and uncertainty assessment within dimensional metrology. To address this, XCT simulation offers a potential solution. While open-source XCT simulation toolkits are commonly used in medical and physical fields, their utilization in industrial geometric metrology remains limited. This study explores the industrial applications of virtual XCT simulation toolkits, focusing on popular open-source options like ASTRA, TIGRE, and gVirtualXray. We analyze configurable input parameters for critical components and summarize potential evaluation metrics for XCT projection image quality.

© 2024 The Authors. Published by Elsevier B.V.
This is an open access article under the CC BY-NC-ND license (https://creativecommons.org/licenses/by-nc-nd/4.0)
Peer-review under responsibility of the scientific committee of the 18th CIRP Conference on Computer Aided Tolerancing

Keywords: Industry X-ray Computed Tomography; Geometric Metrology; X-ray Computed Tomography Simulation;

1. Introduction

X-ray computed tomography (XCT) is widely employed across industries including aerospace, automotive, and medical equipment, due to its capacity for high-resolution non-destructive testing and imaging of intricately manufactured components [1].

According to the ISO 15708-2:2019 standard, industrial CT processes typically involve four main steps: preparation, acquisition, reconstruction, and visualization and analysis, as illustrated in Fig.1. Previous studies have emphasized the uncertainties present in each stage of XCT measurements [2], which could significantly influence the final measurement results. Some scholars have also explored various sources of uncertainty through experiments, such as workpiece placement [3], beam hardening [4], and X-ray exposure [5]. Still, many of these uncertainties are established during the preparation and acquisition stages, with evaluation often conducted after reconstruction, leading to error propagation. Moreover, conducting geometric measurements via XCT experiments is both time-consuming and labor-intensive. Hence, employing simulation methods to directly assess the quality of CT projection images has emerged as an economically efficient alternative.

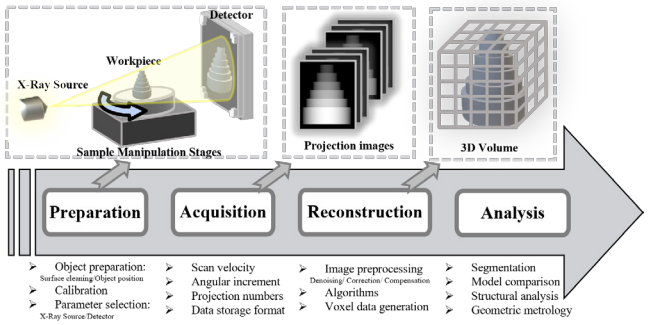

Fig. 1. Process of geometric metrology with XCT

When discussing XCT simulation methods, commercial software and open-source toolkits are the main approaches. In recent years, considerable attention has been given to

2212-8271 © 2024 The Authors. Published by Elsevier B.V.
This is an open access article under the CC BY-NC-ND license (https://creativecommons.org/licenses/by-nc-nd/4.0)
Peer-review under responsibility of the scientific committee of the 18th CIRP Conference on Computer Aided Tolerancing
10.1016/j.procir.2024.10.026

Table 1. Summary of Some XCT commercial software

Name	Institution/Organization	Country	Year
aRTist	BAM	Germany	2007
Scorpius XLab®	Fraunhofer IIS EZRT	Germany	2011
CIVA CT	EXTENDE	France	2008
Novi-Sim	Novitom	France	2017
SimCT	University of Applied Sciences Upper Austria	Austria	2007

commercial software, as listed above in Table 1, such as the Analytical RT Inspection Simulation Tool (aRTist) [6] and Scorpius XLab [7], developed by Berlin Federal Institute for Materials Research and Testing (BAM) and Fraunhofer Institute for Integrated Circuits IIS (EZRT), respectively. Researchers have utilized these tools to explore uncertainties in XCT measurements, including multi-material scenarios [8], penetration length variations [9], surface roughness [10], and detector misalignment [11]. Other notable software includes CIVA [12] and Novi-Sim [13] from France, as well as SimCT [14] from Austria.

Table 2. Summary of Some Mainstream XCT Toolkits

Name	Toolkit Environment		Date
	OS	Compiling Language	
ASTRA [15]	Win/Linux	C++/MATLAB/Python	01/2022
TIGRE [16]	Win/Linux	C++/MATLAB/Python	05/2023
gVirtualXray [17]	Win/Linux/macOS	Python/R/Ruby/Tcl/ C#/Java/GNU/Octave	08/2023
Geant4 [18]	Win/Linux/macOS	C++	05/2023
Syris [19]	Windows	Python	05/2022

"OS" is an abbreviation for Operating System;
Date: The time of the latest version of each toolkit. (MM/YYYY)

Table 2 provides an overview of notable XCT toolkits. The application of open-source XCT simulation toolkits in the industrial domain is steadily expanding. For instance, ASTRA has been utilized to investigate the mitigation of instrument misalignment effects on measurement outcomes [20], as well as to explore automated segmentation methods [21]. Similarly, TIGRE has been employed to study the impact of projection numbers [22, 23] and X-ray exposure times [24] on dimensional metrology. Additionally, the gVirtualXray simulation toolkit accurately reproduces artifact features observed in experimental XCT images [25].

This paper primarily focuses on the exploration of open-source toolkits. Specifically, we analyze and compare the features of three toolkits (ASTRA, TIGRE, and gVirtualXray). Additionally, we delve into reference-based and no-reference image quality assessment metrics for XCT projection images. Metrics calculation is shown on a simple aluminum workpiece.

2. Comprehensive assessment of toolkits functionalities

The X-ray Computed Tomography (XCT) simulation system includes crucial components: the X-ray source, workpiece, sample manipulation stages, and detector, as shown in Fig. 2. These components are essential for imaging. Hence,

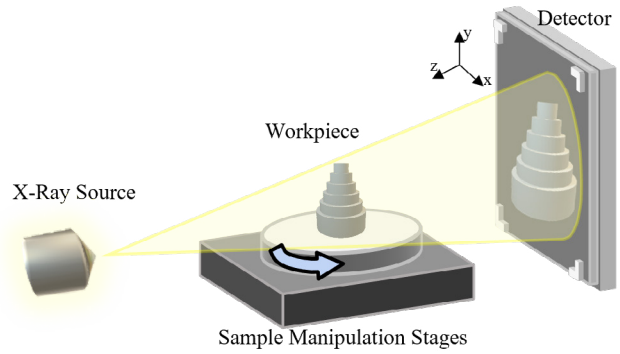

Fig. 2. Schematic diagram of X-ray CT imaging

the following discussion will comprehensively review and compare the three simulation toolkits—ASTRA, TIGRE, and gVirtualXray—focusing on the simulation parameter settings for these components.

2.1. X-Ray Source

The X-ray source generates beams passing through workpieces, essential for acquiring projection images in XCT systems. We analyze its characteristics, including position, shape, and spectrum, as outlined in Table. 3. Additionally, we consider filter features in the simulation toolkit, such as density, thickness, and emission angle, affecting the X-ray beam passing through the workpiece.

Accurate positioning of the X-ray source is essential for achieving precise imaging results. ASTRA and TIGRE allow adjustable positioning relative to workpieces and detectors, gVirtualXray provides precise coordinates (X, Y, Z) for optimal source placement.

For industrial applications, all three simulation toolkits offer options to choose between parallel or cone beam X-ray source shapes. However, ASTRA and TIGRE lack additional customization features. In contrast, gVirtualXray grants additional customization features, such as specifying the cone beam as an infinitesimal point source or a focal spot. Considering the actual focal spot size of an X-ray tube is crucial for an accurate simulation, as X-ray projections are inherently blurred due to temporal inaccuracies (geometric blurring). gVirtualXray allows defining parameters such as size, position, and the number of point sources (N) for the focal spot, simulating geometric blurring by replicating multiple point sources within it. These customization enables accurate simulation of X-ray sources in complex systems, resulting in realistic simulated projection images.

Table 3. Comparison of X-Ray Source Characteristics

Name	X-Ray Source			
	Position	Shape	Spectrum	Filter
ASTRA	Relative	Parallel/Cone	Ideal Mono	×
TIGRE	Relative	Parallel/Cone	Ideal Mono	×
gVirtualXray	Absolute	Parallel/Cone	Mono/Poly	√

Note: In the table, "√" indicates that the toolkit possesses a particular feature, while "×" denotes the absence of that feature.

After selecting the shape of the X-ray source, the next step is to determine the type of beam spectrum: monochromatic or polychromatic. ASTRA and TIGRE simulations use default settings, approximating an ideal monochromatic X-ray source spectrum, gVirtualXray allows users to select and customize monochromatic or polychromatic spectra. In industrial settings, varying photon energies affect material absorption. Low-energy photons may be absorbed, while high-energy ones are more likely to reach the detector. In gVirtualXray, creating a monochromatic or polychromatic beam both requires specifying both the energy and quantity of incident photons.

The source spectrum of industrial XCT machines is typically polychromatic. In front of such tubes, suitable filters are commonly employed to adjust the energy distribution of the beam. Among the toolkits, gVirtualXray empowers users to manually define pertinent parameters using convenient functions such as loadxxxSpectrum($kV, filters, angle$). Users can specify tube voltage (kV), filter composition and thickness, and emission angle. Additionally, it supports the importation of spectra from text documents, simplifying spectrum generation calculation.

Moreover, TIGRE distinguishes itself by its capacity to introduce realistic photon scattering noise, adhering to a Poisson distribution and correlating with the maximum photon count in the detector. This functionality allows users to simulate noise levels.

2.2. Workpiece

When defining workpieces in different simulation software, features as summarized below in Table. 4.

In the exploration process of the ASTRA and TIGRE toolkit, it was found that they require voxel models as input, while gVirtualXRay necessitates mesh models. Mesh models offer higher flexibility in geometric representation, enabling more precise simulation of complex workpieces with intricate internal and external features in industrial applications.

When determining the spatial position of workpieces, it's crucial to define their coordinates (X, Y, Z) and tilt angles. However, ASTRA and TIGRE only offer options to adjust the relative positions of the source and detector, making it challenging to set absolute positions. Moreover, configuring the tilt angle of the workpiece in ASTRA and TIGRE requires users to pre-define it in 3D modeling software before converting it into a voxel model, highlighting a limitation due to the lack of adjustable features within these simulation toolkits. In contrast, gVirtualXRay provides users with the flexibility to specify object coordinates (X, Y, Z) within the simulation coordinate system and set tilt angles along the X, Y, and Z axes after importing the model. This capability enhances the versatility and ease of positioning workpieces in the simulation environment.

After importing the workpiece and establishing its spatial position, the next step is to define its material properties, such as density and composition (element/compound/mixture). ASTRA and TIGRE lack the capability to set material properties, assuming homogeneity during simulation, gVirtualXRay allows for the setting of material, density, and individual components. Moreover, it facilitates the creation of multi-material objects, enabling the assignment of different materials, densities, and chemical compositions to various components, particularly useful for assemblies.

2.3. Sample Manipulation Stages

After configuring the simulation parameters for the X-ray source, object, and detector, determining scanning parameters is essential. These parameters, such as scanning angle, rotation axis, and rotation direction, control the acquisition of projection images, as indicated below in Table. 5.

In ASTRA and TIGRE, users have the flexibility to specify the desired scanning angles to generate corresponding projection images. This flexibility also allows users to customize angle vectors according to specific requirements, including standard linear, sparse, or dense angles. However, currently, parameters for adjusting the rotation axis orientation and direction of the scan have not been found in ASTRA and TIGRE. Nevertheless, it is worth noting that TIGRE allows users to define y-direction displacement for rotation center correction, which can be valuable for studying the uncertainty of rotation axis deviation and its impact on imaging results. While gVirtualXRay requires specifying parameters such as angle step size, total scanning angle or number of projections, rotation axis (e.g., X-axis, Y-axis, or Z-axis), and rotation direction (clockwise-CW or counterclockwise-CCW) to define scanning parameters, providing different methods for angle configuration.

2.4. Detector

The detector serves as a critical component in X-ray CT scanning systems, responsible for receiving X-rays emitted from the source and converting them into signals. In industrial CT simulation, the parameters that need to be defined for the detector mainly fall into two categories: geometric parameters and physical parameters, as shown above in Table. 6.

Geometric parameters like spatial position, detector orientation (upward vector), and geometric calibration (detector

Table 4. Comparison of workpiece characteristics

Name	Workpieces				
	Input	Position	Angle	Density	Matter
ASTRA	Voxel	Relative	×	×	×
TIGRE	Voxel	Relative	×	×	×
gVirtualXray	Mesh	Absolute	√	√	√

Note: In the table, "√" indicates that the toolkit possesses a particular feature, while "×" denotes the absence of that feature.

Table 5. Comparison of sample manipulation stages characteristics

Name	Sample Manipulation Stages		
	Angle	Rotation Axis	Rotation Direction
ASTRA	Arbitrary	×	×
TIGRE	Arbitrary	×	×
gVirtualXray	Angular step	√	√

Note: In the table, "√" indicates that the toolkit possesses a particular feature, while "×" denotes the absence of that feature.

Table 6. Comparison of detector characteristics

Name	Detector				
	Geometric Parameters			Physical Parameters	
	Position	Ori.	Geo. Cal.	Resolution/ Pixel Size	Flatfield Correction
ASTRA	Relative	√	×	√	×
TIGRE	Relative+offset	√	√	√	×
gVirtualXray	Absolute	√	×	√	√

Note: In the table, "Ori." stands for orientation, "Geo. Cal." stands for geometric calibration. "√" indicates that the toolkit possesses a particular feature, while "×" denotes the absence of that feature.

rotation angle) play a crucial role in CT imaging accuracy. ASTRA and TIGRE provide flexibility in configuring detector positions relative to the workpiece. Particularly, TIGRE stands out with an additional feature allowing the offsetting of the detector. This functionality permits adjustments to accommodate the position of the scanned workpiece within the image. In comparison, gVirtualXRay allows for a precise definition of the detector's spatial position, enhancing control over simulation settings. All three software packages include settings for determining the detector orientation (upward vector), ensuring alignment with the desired viewing angle. Regarding geometric calibration, particularly the detector rotation angles (roll-pitch-yaw rotation), TIGRE offers comprehensive adjustments, enabling users to optimize the detector's orientation relative to the scanned workpiece.

Physical parameters include resolution and pixel size. These parameters directly affect the image quality and resolution of CT imaging. All three software packages support customization of these parameters, allowing users to tailor imaging settings according to their specific requirements.

In terms of setting other parameters for projection images, ASTRA currently lacks user-adjustable parameters. TIGRE offers a simplified option to set values for each voxel, improving the accuracy of pixel values on each projection image. Additionally, it approximates detector electronic noise as a Gaussian distribution, allowing users to simulate possible levels of electronic noise and adjust them according to specific simulation requirements. gVirtualXRay stands out for its flat field correction feature. This functionality enables users to calibrate and correct the detector using known scan object materials and input power, mitigating performance degradation caused by fixed pattern noise and ensuring accurate imaging results.

3. Image quality assessment criteria

Given the complexity of CT measurement simulations and the necessity for reliable simulated projection images, subjective visual evaluation alone may not suffice for assessing image quality. Thus, an objective approach using digital image metrics is crucial. These metrics can be categorized into two types: reference-based and no-reference. Here, we summarize evaluation methods suitable for assessing the quality of simulated XCT projection images.

3.1. Reference-based image quality assessment (R-IQA)

Reference-based image quality assessment method compares simulated projection images with actual XCT experimental projection images. This comparison is based on the structures, content, or features of the images, such as intensity values, brightness, contrast, and structural similarity [26]. This section will introduce and analyze some commonly used metrics and their basic calculation principles [27].

Root Mean Square Error (RMSE) is the square root of the mean of the squared differences of pixel intensities between two images.

$$\mathrm{RMSE} = \sqrt{\frac{1}{N}\sum_{i=1}^{N}[I_i - J_i]^2} \tag{1}$$

where N is the number of pixels, I_i and J_i respectively represent the pixel values at position i in two images.

Pearson Correlation Coefficient (CC) quantifies the linear association between two images by evaluating the correlation coefficient of their intensity values. Its mathematical representation is as follows:

$$\mathrm{CC}(I,J) = \frac{\mathrm{cov}\,(I,J)}{\sigma_I \cdot \sigma_J} \tag{2}$$

where $\mathrm{cov}(I,J)$ is the covariance between the intensity values of the two images I and J, and σ_I and σ_J are their respective standard deviations. The coefficient ranges from -1 to 1. In practice, CC values closer to 1 indicate a stronger positive correlation.

Mean Structural Similarity Index (MSSIM) evaluates the similarity between two images concerning luminance $l(I,J)$, contrast $c(I,J)$, and structure $s(I,J)$, aiming to offer a perceptual approximation of image quality [28].

$$\mathrm{MSSIM}(I,J) = \frac{1}{N}\sum_{i=1}^{N}\mathrm{SSIM}(I,J) \tag{3}$$

$$\mathrm{SSIM}(I,J) = [l(I,J)]^{\alpha}\,[c(I,J)]^{\beta}\,[s(I,J)]^{\gamma} \tag{4}$$

where α, β, and γ control the relative importance of three components. N represents the number of localized regions within the image used to evaluate similarity. The formulas for calculating luminance, contrast, and structure similarity are as follows, respectively.:

$$l(I,J) = \frac{2\mu_I \cdot \mu_J + (\mathrm{K_1G})^2}{{\mu_I}^2 + {\mu_J}^2 + (\mathrm{K_1G})^2} \tag{5}$$

$$c(I,J) = \frac{2\sigma_I \cdot \sigma_J + (\mathrm{K_2G})^2}{{\sigma_I}^2 + {\sigma_J}^2 + (\mathrm{K_2G})^2} \tag{6}$$

$$s(I,J) = \frac{2\sigma_{IJ} + (\mathrm{K_2G})^2}{2\sigma_I \cdot \sigma_J + (\mathrm{K_2G})^2} \tag{7}$$

where μ_I and μ_J are the mean pixel intensities of image I and J, σ_I and σ_J are the standard deviations of pixel intensities

of image I and J, K_1 and K_2 is a small constant to avoid instability when the denominator approaches zero, G is the dynamic range of the pixel gray values, for 8-bit grayscale images, pixel values range from 0 to 255. σ_{IJ} is the covariance between pixel intensities of images I and J, given by

$$\sigma_{IJ} = \frac{1}{N-1}\sum_{i=1}^{N}(I_i - \mu_I)\cdot(J_i - \mu_J) \tag{8}$$

MSSIM values closer to 1 indicate higher similarity between images, while the values closer to 0 indicate significant structural differences.

Universal Quality Index (UQI): The UQI assesses the similarity between two images by considering their mean, variance, and covariance [29].

$$\mathrm{UQI}(I,J) = \frac{4\mu_1\cdot\mu_J\cdot\mathrm{cov}(I,J)}{(\mu_I{}^2+\mu_J{}^2)\cdot(\sigma_I{}^2+\sigma_J{}^2)} \tag{9}$$

where μ_I and μ_J are the means, σ_I^2 and σ_J^2 are the variances, and $\mathrm{cov}(I,J)$ is the covariance between the intensity values of the two images I and J. The UQI value ranges from 0 to 1, with higher values indicating greater similarity to the true image.

3.2. No-reference image quality assessment (NR-IQA)

The advantage of NR-IQA metrics lies in their independence from reference experimental XCT projection images during the calculation process. Instead, these methods assess the quality of simulated images solely based on their intrinsic characteristics, such as statistical information, edge details, and other image features. In theory, the closer the numerical values of simulated computational metrics are to those of the actual reference metrics, the better the simulation results are deemed to be.

Signal-to-Noise-Ratio (SNR) was evaluated from different areas in the target region and background region.

$$\mathrm{SNR} = \frac{\mu_t}{\sigma_b} \tag{10}$$

where μ_t is the mean gray value for the target region, typically refers to the region of interest (e.g., the scanned workpiece), and σ_b is the standard deviation of the gray value for the background region, it denotes the surrounding area outside the region of interest, same as followed.

Contrast to Noise Ratio (CNR) evaluates the level of contrast in an image relative to the background noise. The formula is:

$$\mathrm{CNR} = \frac{\mu_t - \mu_b}{\sigma_b} \tag{11}$$

where μ_t and μ_b are the mean gray values for the target and background regions, respectively, and σ_b is the standard deviation of the gray values for the background region.

Contrast over Unsharpness(C/U) assesses the contrast of an image relative to its overall sharpness [30]. The formula is as follows:

$$\mathrm{C/U} = \frac{\mathrm{CNR}}{\mathrm{UNIF}} = \frac{\mu_t - \mu_b}{\sigma_b\cdot\mu} \tag{12}$$

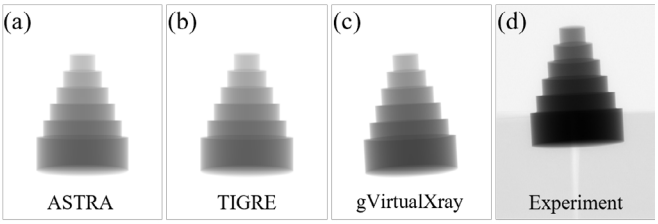

Fig. 3. CT Projection Images - Simulation vs. Experimental (a)ASTRA; (b)TIGRE; (c)gVirtualXray; (d) Measured image

CNR represents the contrast-to-noise ratio, and UNIF stands for the overall uniformity of the entire image, with μ being comprised of both target and background components.

Image Quality Measure (Q) evaluates the difference in grayscale between regions of the target and background in an image relative to their respective noise levels [31]. The formula is given by:

$$Q = \frac{\mu_t - \mu_b}{\sqrt{\sigma_t^2 + \sigma_b^2}} \tag{13}$$

4. Example of metrics calculation

A simple 6 steps multi-diameter aluminum cylinder was considered to illustrate the calculation of the criteria. In this example, we fully utilize the functionalities provided by each toolkit to generate CT projection images. Both experimental and simulated images are depicted in Fig. 3.

Since the simulated images are ideal and generated without background noise, the focus lies on computing a series of reference-based image quality assessment (R-IQA) metrics for the projection images generated by the three simulation toolkits. The results are presented in Table 7, with values retained to four decimal places, where it is noteworthy that the reference images are the projection images obtained from experiments

All simulations exhibit approximate similarity in root mean square error (RMSE) and correlation coefficient (CC) values. However, when considering metrics like universal quality index (UQI), and mean structural similarity index (MSSIM), the computed R-IQA metrics for ASTRA and TIGRE exhibit remarkable similarity, with gVirtualXray displaying slightly higher prediction capability, possibly attributable to parameters within the X-ray source settings.

5. Conclusion and Outlook

This paper provides an initial overview of the research landscape in XCT simulation, exploring and comparing

Table 7. The results of evaluation criteria of CT simulation projection images

Toolkit Name	Images Evaluation Criteria(R-IQA)			
	RMSE	CC	MSSIM	UQI
ASTRA	10.1762	0.6165	0.5535	0.5505
TIGRE	10.1743	0.6163	0.5532	0.5502
gVirtualXray	10.3559	0.6192	0.5939	0.5914

three simulation software packages: ASTRA, TIGRE, and gVirtualXray. It focuses on key components such as the X-ray source, workpiece, sample manipulation stages, and detector, and discusses setting parameters related to XCT measurement uncertainty. Criteria for comparing the toolkits were introduced and then applied to a reference sample.

Moving forward, the plan is to delve deeper into the specific parameters of these XCT simulation toolkits. This will involve considering noise characteristics in the simulation process and aligning simulation parameters with actual experimental conditions to generate different angles of XCT projection images using various toolkits. Subsequently, both reference-based and no-reference image quality assessment metrics will be employed to evaluate the imaging performance of different toolkits, with corresponding angles of experimental projection images serving as benchmarks. This evaluation aims to provide valuable insights for researchers in selecting the most suitable toolkit for their imaging requirements.

Acknowledgements

We gratefully acknowledge the MICS (Made in Italy – Circular and Sustainable) Extended Partnership and received funding from the European Union Next-GenerationEU (Piano Nazionale di Ripresa e Resilienza (PNRR) – Missione 4 Componente 2, Investimento 1.3 – D.D. 1551.11-10-2022, PE00000004).

References

[1] P. Withers, C. Bouman, S. Carmignato, V. Cnudde, D. Grimaldi, C. Hagen, E. Maire, M. Manley, A. Du Plessis, S. Stock, X-ray computed tomography, Nat Rev Methods Primers 1 (2021) 18.

[2] W. Dewulf, H. Bosse, S. Carmignato, R. Leach, Advances in the metrological traceability and performance of x-ray computed tomography, Cirp Ann. 71 (2022) 693–716.

[3] C. Heinzl, J. Kastner, A. Amirkhamov, E. Gröller, C. Gusenbauer, Optimal specimen placement in cone beam x-ray computed tomography, Ndt And E Int. 50 (2012) 42–49.

[4] W. Dewulf, Y. Tan, K. Kiekens, Sense and non-sense of beam hardening correction in ct metrology, Cirp Ann. 61 (2012) 495–498.

[5] H. Villarraga-Gómez, S. Smith, Effect of the number of projections on dimensional measurements with x-ray computed tomography, Precis. Eng. 66 (2020) 445–456.

[6] C. Bellon, A. Deresch, C. Gollwitzer, G.-R. Jaenisch, Radiographic simulator artist: version 2, 18th World Conference on nondestructive testing (2012) 16–20.

[7] S. Reisinger, S. Kasperl, M. Franz, J. Hiller, U. Schmid, Simulation-based planning of optimal conditions for industrial computed tomography, International Symposium on Digital Industrial Radiology and Computed Tomography (2011) 20–22.

[8] F. Borges De Oliveira, M. Bartscher, U. Neuschaefer-Rube, J. Hiller, R. Tutsch, On the importance of multi-material acceptance testing for ct-based cmss, Precis. Eng. 82 (2023) 184–198.

[9] H. Villarraga-Gómez, E. Morse, S. Smith, Assessing the effect of penetration length variations on dimensional measurements with x-ray computed tomography, Precis. Eng. 79 (2023) 146–163.

[10] S. Carmignato, V. Aloisi, F. Medeossi, F. Zanini, E. Savio, Influence of surface roughness on computed tomography dimensional measurements, Cirp Ann. 66 (2017) 499–502.

[11] M. Ferrucci, E. Ametova, S. Carmignato, W. Dewulf, Evaluating the effects of detector angular misalignments on simulated computed tomography data, Precision Engineering 45 (2016) 230–241.

[12] R. Fernandez, L. Clement, D. Tisseur, R. Guillamet, M. Costin, C. Vienne, V. Colombie, Rt modelling for ndt recent and future developments in the civa rt/ct module (2016) 13–17.

[13] A. Autret, A. Sonzogni, O. Guiraud, J. Bourgeas, B. Fayard, Novi-sim: A new fast simulation for x-ray tomography, ICTMS (2017).

[14] M. Reiter, M. Erler, C. Kuhn, C. Gusenbauer, J. Kastner, Simct: a simulation tool for x-ray imaging, Proceedings of the 6th Conference on Industrial Computed Tomography (2016).

[15] W. Van Aarle, W. Palenstijn, J. De Beenhouwer, T. Altantzis, S. Bals, K. Batenburg, J. Sijbers, The astra toolbox: A platform for advanced algorithm development in electron tomography, Ultramicroscopy 157 (2015) 35–47.

[16] A. Biguri, R. Lindroos, R. Bryll, H. Towsyfyan, H. Deyhle, I. Khalil Harrane, R. Boardman, M. Mavrogordato, M. Dosanjh, S. Hancock, T. Blumensath, Arbitrarily large tomography with iterative algorithms on multiple gpus using the tigre toolbox, J. Parallel Distrib. Comput. 146 (2020) 52–63.

[17] F. Vidal, P.-F. Villard, Development and validation of real-time simulation of x-ray imaging with respiratory motion, Comput. Med. Imaging Graph. 49 (2016) 1–15.

[18] S. Agostinelli, J. Allison, K. Amako, J. Apostolakis, H. Araujo, P. Arce, M. Asai, D. Axen, S. Banerjee, G. Barrand, Geant4—a simulation toolkit, Nuclear Instruments and Methods in Physics Research Section A: Accelerators, Spectrometers, Detectors and Associated Equipment 506 (2003) 250–303.

[19] T. Faragó, P. Mikulík, A. Ershov, M. Vogelgesang, D. Hänschke, T. Baumbach, syris: a flexible and efficient framework for x-ray imaging experiments simulation, J. Synchrotron Radiat. 24 (2017) 1283–1295.

[20] E. Ametova, M. Ferrucci, S. Chilingaryan, W. Dewulf, Software-based compensation of instrument misalignments for x-ray computed tomography dimensional metrology, Precis. Eng. 54 (2018) 233–242.

[21] C. Martinez, D. Bolintineanu, A. Olson, T. Rodgers, B. Donohoe, K. Potter, S. Roberts, R. Pokharel, S. Forrest, N. Moore, Automated segmentation of porous thermal spray material ct scans with predictive uncertainty estimation, Comput. Mech. 72 (2023) 525–551.

[22] Z. X. Zhang, S. Lijuan, W. Bo, P. Bing, Effect of the number of projections in x-ray ct imaging on image quality and digital volume correlation measurement, Measurement 194 (2022) 111061.

[23] W. Sun, S. Chretien, A. Biguri, M. Soleimani, T. Blumensath, J. Talbott, The realisation of fast x-ray computed tomography using a limited number of projection images for dimensional metrology, Ndt And E Int. 137 (2023) 102852.

[24] C. Rossides, H. Towsyfyan, A. Biguri, H. Deyhle, R. Lindroos, M. Mavrogordato, R. Boardman, W. Sun, T. Blumensath, Effects of fast x-ray cone-beam tomographic measurement on dimensional metrology, Metrologia 59 (2022) 044003.

[25] F. Vidal, I. Mitchell, J. Létang, Use of fast realistic simulations on gpu to extract cad models from microtomographic data in the presence of strong ct artefacts, Precis. Eng. 74 (2022) 110–125.

[26] A. A. Goshtasby, Similarity and Dissimilarity Measures, Springer, London, 2012, pp. 7–66.

[27] J. Kim, J. Nuyts, A. Kyme, Z. Kuncic, R. Fulton, A rigid motion correction method for helical computed tomography (ct), Physics in Medicine & Biology 60 (5) (2015) 2047.

[28] Z. Wang, A. C. Bovik, H. R. Sheikh, E. P. Simoncelli, Image quality assessment: from error visibility to structural similarity, IEEE transactions on image processing 13 (4) (2004) 600–612.

[29] Z. Wang, A. C. Bovik, A universal image quality index, IEEE signal processing letters 9 (3) (2002) 81–84.

[30] W. Tait, Unsharpness and contrast in digitised images, Physics in Medicine & Biology 27 (9) (1982) 1177–1186.

[31] A. Du Plessis, M. Tshibalanganda, S. Le Roux, Not all scans are equal: X-ray tomography image quality evaluation, Materials Today Communications 22 (2020) 100792.